Orbital response of single-layer antimony to external magnetic field

G. V. Pushkarev,[1] I. A. Iakovlev,[1] D. A. Prishchenko,[1] E. A. Stepanov,[2,1]
V. V. Mazurenko,[1] V. G. Mazurenko,[1] and A. N. Rudenko[3,1,*]

[1]*Department of Theoretical Physics and Applied Mathematics, Ural Federal University, 620002 Ekaterinburg, Russia*
[2]*I. Institute of Theoretical Physics, Department of Physics, University of Hamburg, 20355 Hamburg, Germany*
[3]*Key Laboratory of Artificial Micro- and Nano-Structures of Ministry of Education and School of Physics and Technology, Wuhan University, Wuhan 430072, China*

(Received 30 July 2020; revised 21 September 2020; accepted 22 September 2020; published 12 October 2020)

Single-layer antimony or antimonene is a recently discovered two-dimensional material with high environmental stability and appealing electronic properties. Antimonene is characterized by strong spin-orbit coupling, which suggests unconventional behavior in magnetic fields. In this paper, we report on a computational study of the magnetic response of antimonene focusing on the effect of gate voltage, playing an important role due to the buckled structure of antimonene. We use a tight-binding model and systematically analyze the magnetic susceptibility as well as Landau quantization of the energy spectrum. We show that the magnetic response of undoped antimonene is diamagnetic, similar to its bulk phase. In contrast, for electron-doped antimonene we observe a paramagnetic response, which can be further reversed if the vertical bias voltage is applied. The mechanism of the observed switching is related to a modulation of the orbital susceptibility due to the spin splitting occurring as a result of electric-field-induced inversion symmetry breaking. From the calculated Landau levels, we find a significant difference between the g-factors for electrons ($g_e \approx 2.33$) and holes ($g_h \approx 6.48$), which also exhibit a strong dependence on the bias potential.

DOI: 10.1103/PhysRevB.102.155412

I. INTRODUCTION

Since the experimental discovery of graphene [1], the field of two-dimensional (2D) materials has been growing rapidly. These materials have attracted enormous interest from the scientific community due to their unique properties. The variety of 2D materials known today is very diverse, encompassing a broad spectrum of physical properties. Apart from semimetallic graphene and its group-IV analogs, such as silicene [2] and germanene [3,4], a large class of 2D materials is represented by semiconductors, with the most known examples being molybdenum disulfide [5–7] and black phosphorus [8]. Materials with intrinsic magnetic order are a recent addition to the family of 2D materials [9,10]. Of particular interest are 2D materials based on heavy elements as they demonstrate strong spin-orbit (SO) coupling. In magnetic 2D materials, SO coupling is crucially important for thermal stabilization of long-range magnetic order by inducing magnetic anisotropy [11–13]. In nonmagnetic materials, strong SO coupling opens up the possibility to realize topological states and unconventional transport properties [14,15]. Among the elemental materials with strong SO coupling, 2D allotropes of bismuth [16] and antimony [17] can be distinguished.

Single-layer antimony (SL-Sb) is an elemental 2D material (also known as antimonene), which was recently obtained experimentally under ambient conditions [17–22]. SL-Sb is an indirect-gap semiconductor with an energy gap in the near-infrared spectral range. High environmental stability and high carrier mobility make this material a promising candidate for electronic, transport, and optical applications [23–26]. In comparison to other stable 2D materials, SL-Sb features strong SO coupling, which is of potential interest for spintronics [27] and topological applications [28,29]. Recent theoretical studies on the electronic properties of SL-Sb also demonstrate the importance of strong SO coupling for a proper description of this material [30–34]. Interestingly, the combination of strong SO coupling and bias-induced inversion symmetry breaking can lead to a controllable modification of the SL-Sb electronic and optical properties [32,33], as a consequence of the Rashba effect [35]. In this context, the behavior of SL-Sb in magnetic fields constitutes an interesting yet unsolved question.

The primary objective of this work is to study the magnetic response of SL-Sb to an external magnetic field. To this end, we utilize two complementary approaches. The first one is based on a modification of hopping integrals within the tight-binding (TB) formalism according to the field-induced phase factor (Peierls substitution), which is applied here to model magnetic fields with moderate strength [36]. This method can be routinely applied to 2D materials if a reliable TB model is available. Up to now, it has been used to investigate the spectrum of Landau levels in many 2D materials including graphene, phosphorene, MoS_2, and other systems [37–43]. The second approach is based on the calculation of magnetic susceptibility using the perturbation theory with respect to magnetic field and is applicable in the regime of weak fields. Among 2D materials, this kind of method has been previously

*a.rudenko@science.ru.nl

applied to graphene [44] and transition-metal dichalcogenides [45]. As for antimonene, the problem of magnetic response of this material remains unsolved. At the same time, the magnetic response of 2D materials with strong SO coupling is an issue of fundamental interest.

From a computational point of view, the problem of orbital magnetic susceptibility calculation is complicated. The theory of diamagnetism of a free-electron gas was first proposed by Landau in 1930 [46]. The next step was taken by Peierls [47], who derived an expression for the magnetic susceptibility of electrons with an arbitrary dispersion law. It was suggested that the leading contribution to the susceptibility is related to the Fermi-surface curvature. Despite a number of important results, the applicability of this approach was limited to the case of a single-band system. Several attempts were made thereafter to generalize the Landau-Peierls theory to the multiband case [48–52]. However, no exact solution to the problem has been found, while the proposed methods were cumbersome and often lacked a physical interpretation. Notable progress was made by Fukuyama [53], who obtained a relatively simple formula for the orbital susceptibility based on the perturbation theory. In spite of the fact that this method does not recover the Landau-Peierls formula in the case of single-band systems, it was capable of describing a number of interesting effects in multiband systems with strong SO coupling, such as bismuth [54,55]. In the past decade, an alternative computationally tractable approach to the problem of orbital susceptibility was proposed, which is based on a combination of the perturbation theory and the Green's function formalism [56–58]. This approach relies on a TB description, and it allows one to describe the interband effects on magnetic susceptibility in weak fields.

In this paper, we perform a systematic theoretical analysis of the magnetic response in SL-Sb. For this purpose, we use a TB approach [36] in conjunction with a perturbation theory for the susceptibility [56]. We also explicitly consider Landau quantization of the SL-Sb energy spectrum, and we examine the effect of external bias potential, which turns out to be important due to the buckled structure of antimonene. Our findings show that the net magnetic response of undoped SL-Sb is diamagnetic. In contrast, electron-doped SL-Sb demonstrates a paramagnetic behavior with the susceptibility controllable by the external bias potential. We also find that a static electric field applied perpendicular to the surface leads to a significant modification of the Landau levels in SL-Sb, especially for electrons. Electron and hole g-factors are found to be considerably different from each other, and they demonstrate sensitivity to the bias potential.

The rest of the paper is organized as follows. In Sec. II, we present the theory and computational details of the numerical calculations presented in this paper. We then describe the electronic structure of SL-Sb in the presence of the gate voltage (Sec. III A). In Sec. III B, we systematically analyze the magnetic susceptibility of SL-Sb by decomposing it into different physically distinct contributions. Bias-dependent Landau quantization of the SL-Sb energy spectrum, as well as our estimation of the g-factor, are presented in Sec. III C. In Sec. IV, we summarize our results and conclude the paper.

II. MODEL AND COMPUTATIONAL DETAILS

A. Model Hamiltonian

In our calculations, we consider the TB model proposed for SL-Sb in Ref. [31], proven to be suitable for a comprehensive analysis of the electronic properties. The model captures the SO coupling and allows one to take the effect of gate voltage into account [32]. The effective Hamiltonian for SL-Sb can be written as

$$H = H_0 + \sum_{jmn}\sum_{pq} T^{(k_j)}_{mp} h^j_{pq} T^{(k_j)}_{nq} + \frac{V_{\text{bias}}}{d}\sum_{im} z_i c^\dagger_{im} c_{im}, \quad (1)$$

where

$$H_0 = \sum_{mn}\sum_{ij} t^{mn}_{ij} c^\dagger_{im} c_{jn} \quad (2)$$

is the spin-independent part, with t^{mn}_{ij} being the effective hopping parameter between m and n orbitals at atoms i and j, respectively, and $c^\dagger_{im}$ (c_{jn}) is the creation (annihilation) operator of electrons at atom i (j) and orbital m (n). The second term in Eq. (1) describes the SO coupling, where $T^{(k_j)}$ is a sublattice-dependent matrix with k_j being the sublattice index of atom j, which determines the unitary transformation between the basis of cubic harmonics (p atomic orbitals) and the basis of the Wannier functions in which the spinless Hamiltonian H_0 is determined [31]. h^j is the intra-atomic SO Hamiltonian for atom j defined in the basis of p orbitals as (the orbital indices are implicit)

$$h^j = \lambda \sum_{\sigma\sigma'} i\left(c^{\sigma\dagger}_z \sigma^x_{\sigma\sigma'} c^{\sigma'}_y + c^{\sigma\dagger}_z \sigma^y_{\sigma\sigma'} c^{\sigma'}_x + c^{\sigma\dagger}_y \sigma^z_{\sigma\sigma'} c^{\sigma'}_x\right), \quad (3)$$

where λ denotes the intra-atomic SO coupling constant, σ, σ' run over the spin-up and spin-down projections, and $\sigma^{x(y,z)}$ are the Pauli matrices. The last term in Eq. (1) describes the effect of the bias potential, where z_i is the z component of the position operator for atom i, V_{bias} is the magnitude of the bias voltage, and d is the vertical displacement between the sublattices.

B. Magnetic response in weak fields

On the basis of the presented model, we first consider the magnetic response of the system in weak magnetic fields. It can be quantified by the static magnetic susceptibility, which in general can be expressed as the second derivative of the thermodynamic potential Ω with respect to magnetic field B:

$$\chi_{\text{tot}} = -\frac{\mu_0}{S}\frac{\partial^2 \Omega}{\partial B^2}\bigg|_{B\to 0}, \quad (4)$$

where μ_0 is the magnetic permeability constant, S is the sample area, and $\Omega = -T\sum_{n\mathbf{k}} \ln\{1 + \exp[(\mu - E_{n,\mathbf{k}})/T]\}$ is the grand potential, with μ being the chemical potential, and $E_{n,\mathbf{k}}$ is the electron energy at band n and wave vector $\mathbf{k}$. In principle, Ω can be calculated within the TB approach from the electronic spectrum in magnetic field $E_{n,\mathbf{k}}$. However, this is a computationally very demanding task, especially at weak fields. To circumvent this issue, perturbative approaches are utilized, expanding Ω (or its derivatives) in powers of B-related quantities.

For the present consideration, it is convenient to represent the susceptibility as a sum of spin and orbital terms:

$$\chi_{\text{tot}} = \chi_{\text{spin}} + \chi_{\text{orb}}. \tag{5}$$

The spin part of the susceptibility can be approximated by the susceptibility of free electrons (Pauli paramagnetism) [59]:

$$\chi_{\text{spin}} = \mu_0 \mu_{\text{B}}^2 g(E_{\text{F}}), \tag{6}$$

where $g(E_{\text{F}}) = \sum_{n,\mathbf{k}} \delta(E_{n,\mathbf{k}} - E_F)$ is the density of states (DOS) at the Fermi energy E_F, and μ_{B} is the Bohr magneton.

The orbital susceptibility can be expressed as a sum of two distinct terms, namely the band and the core electron contributions,

$$\chi_{\text{orb}} = \chi_{\text{band}} + \chi_{\text{core}}. \tag{7}$$

In the weak fields, χ_{band} can be calculated perturbatively using the Green's function formalism as it is proposed, e.g., in Refs. [56,60]:

$$\chi_{\text{band}} = -\frac{\mu_0 e^2}{12\hbar^2} \frac{\text{Im}}{\pi S} \int_{-\infty}^{+\infty} n_F(E) \text{Tr}[U_k(E) - 4V_k(E)] dE. \tag{8}$$

Here, e and $\hbar$ are the elementary charge and the Planck constant, respectively. $n_F = [\exp(\frac{E-\mu}{k_B T}) + 1]^{-1}$ is the Fermi-Dirac distribution function, and $\text{Tr}[A(\mathbf{k})] = (N_k)^{-1} \sum_{i,\mathbf{k}} A_{ii}(\mathbf{k})$. $U_k = GH^{xx}GH^{yy} - GH^{xy}GH^{xy}$ and $V_k = GH^xGH^xGH^yGH^y - GH^xGH^yGH^xGH^y$ are matrices, with

$$G(E, \mathbf{k}) = [E\mathcal{I} - H(\mathbf{k}) - i\delta\mathcal{I}]^{-1} \tag{9}$$

being the Green's function matrix, where E denotes energy, $\mathcal{I}$ is the unity matrix, and δ is an infinitesimal parameter playing the role of the Lorentzian smearing in numerical calculations. In the equations above, H^α and $H^{\alpha\beta}$ denote the first and second derivatives of the Hamiltonian with respect to k_α and k_β, which can be calculated analytically in $\mathbf{k}$ space as

$$H^\alpha(\mathbf{k}) = \frac{dH(\mathbf{k})}{dk_\alpha} = \sum_j i r_{j\alpha} H(\mathbf{r}_j) e^{i\mathbf{k}\cdot\mathbf{r}_j} \tag{10}$$

and

$$H^{\alpha\beta}(\mathbf{k}) = \frac{dH(\mathbf{k})}{dk_\alpha dk_\beta} = -\sum_j r_{j\alpha} r_{j\beta} H(\mathbf{r}_j) e^{i\mathbf{k}\cdot\mathbf{r}_j}, \tag{11}$$

where $H(\mathbf{r}_j)$ is the Hamiltonian matrix in real space, and $r_{j\alpha}$ is the α component of the radius vector $\mathbf{r}_j$ corresponding to atom j. The calculations are performed with a primitive cell containing two Sb atoms [31], resulting in a (12×12) Hamiltonian matrix in $\mathbf{k}$-space. To calculate the orbital susceptibility, we use a (750×750) $\mathbf{k}$-point grid, a smearing of $\delta = 0.01$ eV in the Green's function calculations, and we performed the integration over energy with an energy step of $dE = 0.005$ eV.

One can additionally separate the interband χ_{inter} from the intraband contribution χ_{intra} by using the Landau-Peierls formula, which describes the intraband susceptibility:

$$\chi_{\text{intra}} = -\frac{\mu_0 e^2}{12\hbar^2} \sum_n \int_{\text{BZ}} n'_F(E_{n,\mathbf{k}}) \times \left(E^{xx}_{n,\mathbf{k}} E^{yy}_{n,\mathbf{k}} - E^{xy}_{n,\mathbf{k}} E^{xy}_{n,\mathbf{k}}\right) d\mathbf{k}. \tag{12}$$

Here, n is the band index, $n'_F(E_{n,\mathbf{k}})$ is the derivative of Fermi-Dirac distribution with respect to $E_{n,\mathbf{k}}$, and $E^{xx}_{n,\mathbf{k}}$, $E^{yy}_{n,\mathbf{k}}$, $E^{xy}_{n,\mathbf{k}}$ are the second derivatives of the electron dispersion with respect to components of the wave vector. To calculate the derivatives in Eq. (12), we use the finite-difference method. The intraband contribution given by Eq. (12) neglects all interband transitions, and it is the exact solution in the case of a single-band model. Having calculated χ_{intra}, the interband term can be estimated as $\chi_{\text{inter}} = \chi_{\text{band}} - \chi_{\text{intra}}$.

Since Sb is a heavy element, it is also instructive to take the contribution of core electrons into account when calculating the susceptibility. This can be done in the spirit of Langevin diamagnetism theory applied to closed-shell atoms [59]. Specifically, we use the following expression for the susceptibility of core electrons in SL-Sb:

$$\chi_{\text{core}} = -\frac{\mu_0 e^2 n}{6 S m_e} \sum_i Z_i \langle r_i^2 \rangle, \tag{13}$$

where m_e is the free-electron mass, S is the unit cell area, $n = 2$ denotes the number of atoms in the unit cell, $\langle r_i^2 \rangle$ is the mean-square distance of the i-shell electrons from the nucleus, and Z_i denotes the number of electrons in the i shell. To obtain the mean-square distance, we perform an evaluation of Wannier functions (WFs) $\phi_i(\mathbf{r})$ associated with the orbitals of a single Sb atom in real space. The corresponding quantity is then calculated as the expectation value of the r^2 operator in the $\phi_i(\mathbf{r})$ state:

$$\langle r_i^2 \rangle = \int \phi_i(\mathbf{r}) r^2 \phi_i^*(\mathbf{r}) d\mathbf{r}. \tag{14}$$

The WFs $\phi_i(\mathbf{r})$ are obtained from the density functional theory (DFT) calculations using the projected augmented wave method [61] as implemented in the *Vienna ab initio simulation package* (VASP) [62,63], combined with the WANNIER90 package. The calculations were performed within the Perdew-Burke-Ernzerhof (PBE) exchange-correlation functional [64], and they were checked to be fully converged with respect to the numerical parameters. The following orbital contributions to $\langle r_i^2 \rangle$ and $\langle x_i^2 \rangle$ were considered: $4s$, $4p$, $4d$, $5s$, and $5p$ (see Table I), assuming that inner orbitals provide a negligible contribution to the susceptibility. Since $5s$ and $5p$ orbitals participate in the band formation captured by the TB model, their contribution was excluded from χ_{core}.

TABLE I. Mean-square values $\langle r_i^2 \rangle$ and $\langle x_i^2 \rangle$ obtained for the relevant orbitals of a single Sb atom shown along with their contribution to the susceptibility. χ_{atom} is an estimate of the single Sb atom susceptibility given per unit area of an atom in SL-Sb.

Orbital	$\langle r_i^2 \rangle$ (Å^2)	$\langle x_i^2 \rangle$ (Å^2)	Contribution to χ (χ_0)
$4s$	0.177	0.059	−0.11
$4p$	0.331	0.110	−0.22
$4d$	0.602	0.201	−0.39
$5s$	1.626	0.542	−0.64
$5p$	2.824	0.941	−1.11
$4spd$	1.110	0.370	−0.72 (χ_{core}/n)
$4spd$+$5sp$	5.560	1.483	−2.47 (χ_{atom})

For the sake of convenience, we use the following units for 2D susceptibility throughout the paper as proposed in Ref. [56]: $\chi_0 = \mu_0 e^2 \hbar^{-2} a^2 t$ with $t = 1$ eV and $a = 1$ Å. The chosen units correspond to $\chi_0 \sim 4.65 \times 10^{-5}$ Å ($\sim 2.05 \times 10^{-10}$ m^3/mol in SI units). In these units, the contribution of core electrons to the susceptibility of SL-Sb is $\chi_{\text{core}} = -0.72\chi_0$ per Sb atom.

C. Landau quantization

To examine the magnetic response of SL-Sb in moderate fields, we study the Landau quantization of the energy spectrum. To this end, we calculate the Landau levels in terms of the TB model, which requires a modification of the hopping integrals according to the Peierls substitution [36]:

$$t_{ij}^{mn} \to t_{ij}^{mn} e^{\gamma_{ij}}, \tag{15}$$

$$\gamma_{ij} = -2\pi i \frac{e}{\hbar} \int_{r_i}^{r_j} \mathbf{A} \cdot d\mathbf{l}, \tag{16}$$

where $\mathbf{A}$ is the vector potential of the electromagnetic field. For a homogeneous perpendicular magnetic field B_z applied along the z direction, we choose the Landau gauge $\mathbf{A} = (0, B_z x, 0)$. Thus, the additional phase factor will have the following form [42,65]:

$$\gamma_{ij} = -2\pi i \frac{e}{h} B_z \frac{1}{2}(x_i + x_j)(y_i - y_j). \tag{17}$$

To evaluate γ_{ij}, we introduce a coordinate grid as shown in Fig. 1. The grid is defined as $x_a + n \equiv n(\sqrt{3}/2a)$, $y + n \equiv n(1/2a)$, and $x_b + n = x_a + n + a/\sqrt{3}$, where $x_{a(b)}$ is the x coordinate of atoms belonging to the sublattice A (B), a is the lattice parameter, and n numerates unit cells in the constructed supercell. Using such a coordinate grid, one can easily evaluate the additional phase factors to the hopping parameters using Eq. (17). For example, for the vector $\mathbf{R} = (-1/2\sqrt{3}, 1/2)a$, we have

$$\gamma_{ij} = -\pi i \frac{\Phi}{\Phi_0}\left(n - \frac{1}{6}\right), \tag{18}$$

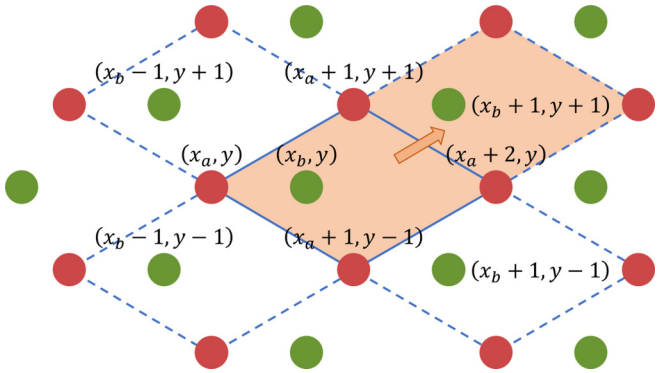

FIG. 1. Schematic representation of the coordinate cell introduced to calculate the Landau levels. The unit cell is bounded by the solid lines. The shaded area corresponds to an example of the supercell constructed to consider variable surface area, which determines the magnetic flux. Atoms belonging to the sublattices A and B with the lattice parameter a are shown by red and green circles, respectively.

where $\Phi = B_z a^2 \sqrt{3}/2$ is the magnetic flux through the unit cell and $\Phi_0 = h/e$ is the magnetic flux quanta.

Due to the fact that magnetic flux through the unit cell is quantized, we consider a supercell composed of q unit cells, such that $\Phi = \Phi_0/q$. This means that the dimensionality of the TB Hamiltonian increases as B decreases. In our calculations, we have increased the size of the unit cell in the direction depicted in Fig. 1 by an arrow. The way to construct the Hamiltonian and impose periodic boundary conditions is described, e.g., in Ref. [40]. The Landau levels are obtained by diagonalizing the Hamiltonian at the center of the Brillouin zone (Γ-point) for each magnetic flux (supercell size) considered.

To calculate the g-factors, we add the Zeeman term to the Hamiltonian Eq. (1) in the following form:

$$H_z = -\frac{1}{2} g_s \mu_B B_z \sum_{im} \sum_{\sigma\sigma'} c_{im}^{\sigma\dagger} \sigma_{\sigma\sigma'}^z c_{im}^{\sigma'}, \tag{19}$$

where $g_s = 2$ is the g-factor of an electron. This term contributes to the energy splitting of the Landau levels $\Delta E = g\mu_B B_z$, corresponding to up and down spin projections, from which one can determine the effective g factor. Without SO coupling, $g = g_s$, whereas g becomes dependent on the constant λ if SO coupling is present.

III. RESULTS AND DISCUSSION

A. Electronic structure

Single-layer Sb adopts a buckled honeycomb structure (point group D_{3d}) with the lattice parameter $a = 4.12$ Å and two sublattices vertically displaced by $d = 1.65$ Å. The corresponding crystal structure is schematically shown in Fig. 2(a), with the Brillouin zone in Fig. 2(b). The band structure of SL-Sb calculated for the bias potentials $V_{\text{bias}} = 0.0$ and $V_{\text{bias}} = 1.5$ eV is presented in Fig. 2(c). In the absence of external fields, the electronic structure features an indirect band gap of $\sim$0.9 eV with the valence-band maximum located at the

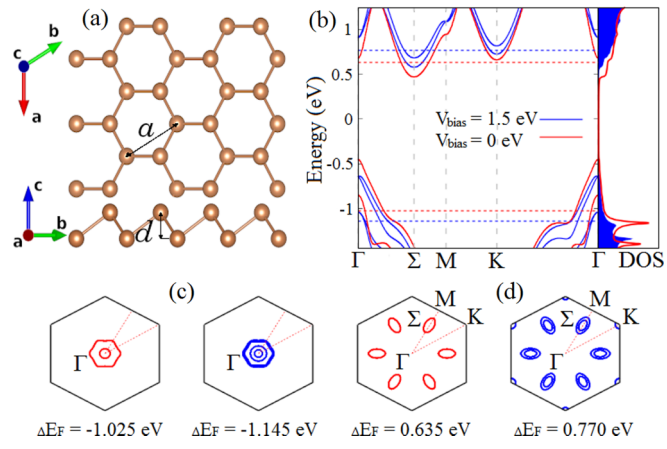

FIG. 2. (a) Schematic atomic structure of SL-Sb with top and side views. (b) Band structure and DOS calculated for two different values of the bias potential. Zero energy corresponds to the center of a band gap. (c) and (d) show the Fermi contour around the band edges for holes and electrons, respectively. The red and blue color correspond to $V_{\text{bias}} = 0.0$ and 1.5 eV, respectively.

Γ-point and the conduction-band minimum located at the Σ-point along the Γ-M direction of the Brillouin zone. Due to the presence of inversion symmetry in SL-Sb, the electronic bands are doubly degenerate with respect to the spin degrees of freedom. This degeneracy is lifted when the inversion symmetry is broken, i.e., in the presence of an external electric field normal to the SL-Sb surface. The degree of the resulting band splitting is dependent on the gate voltage, which opens up the possibility for a controllable modification of the transport and optical properties of SL-Sb [32,33]. In the context of the magnetic response, we expect that the transitions emerging due to the band splitting will contribute to the orbital susceptibility, as well as affect the Landau levels. It is also worth noting that the effect of a vertical electric field induces a slight enhancement of the band gap.

Figures 2(c) and 2(d) show the Fermi surfaces of hole- and electron-doped SL-Sb with the carrier concentration of $n = 1 \times 10^{14}$ cm^{-2}. From Fig. 2(c), one can see that the hole Fermi surface forms a circle around the Γ-point. When the bias voltage is applied, the Fermi surface splits into two concentric circles as a result of the spin splitting. The situation with the electron states is different. In this case [Fig. 2(d)], the conduction-band minimum is located at the Σ-point, forming six valleys around the zone center. Each pocket of the Fermi surface is slightly anisotropic and has an elliptical shape. Similar to the hole case, each pocket splits into two ellipses if the bias potential is applied. Considering a pronounced modification of the band structure and the Fermi surface, one can expect a variation of the orbital part of the magnetic response in SL-Sb with respect to the bias voltage.

B. Magnetic susceptibility

In Fig. 3, we show three distinct contributions to the orbital susceptibility: χ_{inter}, χ_{intra}, and χ_{core} calculated as a function of the chemical potential for different bias voltages. One can see that the interband contribution is paramagnetic ($\chi > 0$) for most of the chemical potentials considered. In contrast, the intraband contribution is mostly diamagnetic ($\chi < 0$). This is consistent with the Landau-Peierls theory, predicting diamagnetism for systems with effective masses of carriers such that $m < 1/\sqrt{3}m_0$, which is fulfilled in SL-Sb [31]. In doped SL-Sb, the interband contribution is always larger, resulting in the net paramagnetic response, and emphasizing the importance of the interband effects in the susceptibility. On the other hand, core electrons provide a significant diamagnetic response that is approximately five times larger than the band susceptibility in the gap region. When the bias voltage is applied, the shape of the orbital susceptibility changes as a result of the spin splitting. This leads to a reduction of the intra and interband contributions.

From Fig. 3, one can see that the application of a sizable bias voltage changes χ_{inter} near the valence-band edge from paramagnetic to strongly diamagnetic. In this case, χ_{intra} and χ_{inter} terms are summed up rather than compensate each other, leading to a pronounced diamagnetic peak. On the other hand, as far as the conduction band is concerned, neither χ_{intra} nor χ_{inter} changes its behavior, and they remain diamagnetic and paramagnetic, respectively. Within the energy gap, the interband susceptibility is decreased when the bias voltage is applied, even demonstrating a transition from paramagnetic to diamagnetic response at $V_{\text{bias}} = 1.5$ eV. Nevertheless, the susceptibility of undoped SL-Sb is almost exclusively determined by the diamagnetic core contribution, which is bias-independent.

The total magnetic susceptibility of SL-Sb, along with the orbital and spin contributions, is shown in Fig. 4. In the gapped region the spin susceptibility vanishes, making the orbital response the only factor determining the total magnetic susceptibility in undoped SL-Sb. In this case, the resulting susceptibility is diamagnetic with $\chi \approx -1.0\chi_0$. If the bias voltage is applied, this value changes slightly, reaching $\chi \approx -1.4\chi_0$ at $V_{\text{bias}} = 1.5$ eV. By magnitude, such a response is comparable with the diamagnetic response of water [66]. In absolute values, the orbital response is an order of magnitude larger than the paramagnetic plateau in graphene [44,45,56].

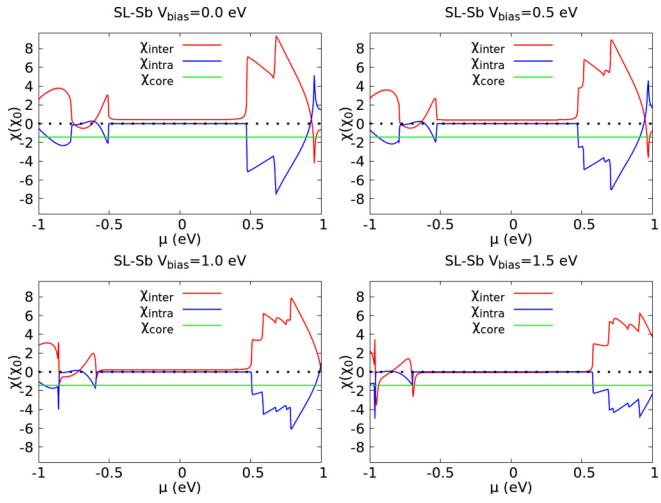

FIG. 3. Individual interband (χ_{inter}), intraband (χ_{intra}), and core electron (χ_{core}) contributions to the orbital part of magnetic susceptibility (χ_{orb}) of SL-Sb calculated as a function of the chemical potential μ for different values of the bias voltage V_{bias}.

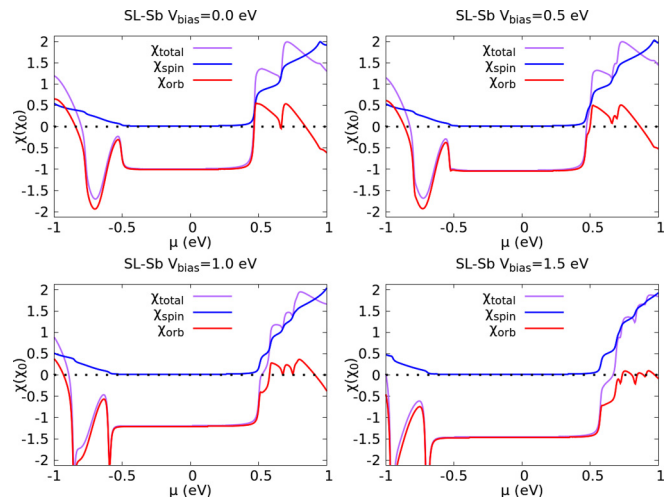

FIG. 4. Total magnetic susceptibility of SL-Sb calculated as a function of the chemical potential μ for different values of the bias voltage V_{bias}.

It is worth noting that for bulk Sb crystal the magnetic response is also diamagnetic with the experimental value $\chi_{exp} \approx -1 \times 10^{-4}$ cm^3/mol [67,68], which can be translated into $\sim -6.0\chi_0$, meaning that the magnetic response in SL-Sb is an order of magnitude smaller. This can be attributed to the metallic behavior of bulk Sb, giving rise to a nonzero intraband contribution to the susceptibility.

Interestingly, electron-doped SL-Sb demonstrates a paramagnetic behavior as can be seen from Fig. 4. Spin contribution in the conduction-band region is comparably large and gives a strong paramagnetic contribution for every V_{bias} considered. Nevertheless, the total susceptibility for the case of light electron doping can be effectively reduced by increasing the bias voltage. Moreover, the application of a large enough bias voltage leads to a sign change in the total susceptibility for the above-mentioned case, making the net response diamagnetic. In contrast, the total susceptibility of hole-doped SL-Sb is diamagnetic. The bias voltage does not change the diamagnetic behavior, yet at $V_{\text{bias}} \gtrsim 1.0$ eV one can see the formation of a diamagnetic divergence at the valence-band edge. It is worth noting that strong electric fields may be required to realize such bias voltage in SL-Sb, which is quite challenging experimentally. Possible ways to overcome this issue include, for example, interface engineering with polar semiconductors [69], or heavy doping by alkali metals [70].

C. Bias-dependent Landau levels

To study the influence of moderate magnetic fields on the electronic spectrum of SL-Sb, we consider the first Landau levels for electrons and holes in the presence of the bias potential. We perform calculation with the SO coupling constant $\lambda = 0.34$ eV, which is consistent with the intra-atomic SO strength of neutral Sb atoms [71] and was used in previous TB studies of SL-Sb [31,32]. As can be seen from Fig. 5(a), for electron-doped SL-Sb the gating leads to the formation of a gap between upper and lower bands even at zero magnetic field, in agreement with the band structure shown in Fig. 2(c). One can also see that the position of the Landau levels on the energy scale depends on V_{bias}, which is again related to the corresponding position of the conduction-band minimum. All the electronic levels accurately follow a linear dependence as a function of the magnetic field. In contrast, the hole levels exhibit a deviation from the linear dependence at $B_z > 20$ T, suggesting the presence of high-order terms in B_z [Fig. 5(b)]. Also, in the case of holes, there is no energy gap at zero

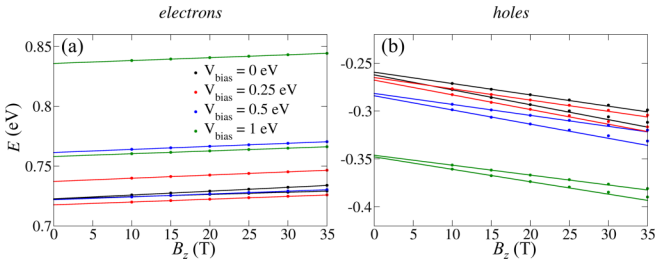

FIG. 5. First Landau levels calculated for (a) electrons and (b) holes in SL-Sb using different values of V_{bias}. Lines are obtained from the linear regression.

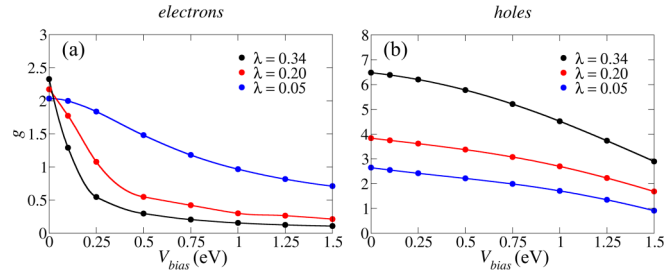

FIG. 6. Dependence of the calculated g-factor on the bias potential V_{bias} for (a) electrons and (b) holes in SL-Sb using various values of the SO coupling constant λ. Curves are obtained using Akima splines.

field, which can be attributed to a high-symmetry position of the valence-band minimum. The obtained dependencies can be used to estimate the bias-dependent g-factors for electrons and holes in SL-Sb. We note that the presence of nonlinear terms in the Landau fan diagram for holes means that the corresponding g-factor is field-dependent. However, since the deviation at moderate fields below 35 T is not significant, we neglect the mentioned nonlinearity and fit the energy levels by linear functions, i.e., as $E^{\pm}(B_z) = e_0 \pm g\mu_B B_z/2$.

We find that the g-factors of electrons and holes are significantly different from each other. Even without external bias field, we obtain $g_e \approx 2.33$ and $g_h \approx 6.48$. When we increase the bias voltage slightly, g_e decreases rapidly and tends to $\approx$0.1 at $V_{\text{bias}} = 1.5$ eV, as is shown in Fig. 6(a). In the case of holes [Fig. 6(b)], g_h remains almost unaffected by small bias voltages, and it decreases linearly after $V_{\text{bias}} \approx 0.75$ eV, approaching $g_h \approx 3.0$ at $V_{\text{bias}} = 1.5$ eV. Therefore, strong SO coupling in SL-Sb significantly affects its hole g-factor, whereas both electron and hole g-factors can be effectively tuned by an external electric field. Overall, both g_e and g_h decrease with V_{bias}, which is consistent with the behavior of orbital susceptibility (Sec. III B), tending to be diamagnetic at increasing V_{bias}.

To gain more insight into the behavior of g factors, we consider two additional values of the SO coupling constants $\lambda = 0.2$ and 0.05 eV, which correspond to the intra-atomic SO coupling in arsenic (As) and phosphorus (P) [71], whose 2D phases have electronic and crystal structures similar to antimony [72]. As expected, for decreasing λ the factors g_e and g_h tend to the value of 2 irrespective of the applied bias. Importantly, even for small λ one can see a notable deviation of the g-factor from 2 at large V_{bias}, meaning that similar effects could be observed in SL-As and SL-P. As for the dependence g versus V_{bias}, the overall behavior does not change significantly either for electrons or for holes, as can be seen from Fig. 6. However, the SO coupling leads to a smaller splitting of the Landau levels for electrons at increasing bias, thus g_e becomes less sensitive to V_{bias} at small λ.

IV. CONCLUSION

In this paper, we have systematically studied the magnetic response of SL-Sb in weak and in moderate fields using the TB formalism including the SO coupling and external bias potential. Our results show that undoped SL-Sb

demonstrates a diamagnetic response, which is about one order of magnitude smaller than in its bulk counterpart. In contrast, electron-doped SL-Sb is found to be paramagnetic with the susceptibility controllable by the external electric field. At large enough fields and light dopings, the susceptibility can even be switched to the diamagnetic one. The paramagnetic behavior is attributed to the relatively large spin susceptibility at the conduction-band edge, which is compensated by the orbital susceptibility if the bias voltage is applied. In turn, the switching mechanism is mainly related to the suppression of interband susceptibility as a result of the bias-induced spin splitting of energy bands.

Additionally, we examined the Landau levels for electrons and holes in SL-Sb, which allowed us to estimate the bias-dependent g-factors. We find that the g-factors for electrons and holes are significantly different from each other, yielding $g_e \approx 2.33$ and $g_h \approx 6.48$, respectively, without external bias. If the bias voltage is applied, the g-factors are reduced significantly in both cases, but they remain positive for any meaningful bias potentials. Despite significantly weaker SO coupling, we expect qualitatively similar results in isostructural phases of SL-As and SL-P. Thus, our results can motivate further experimental studies of group-V 2D hexagonal semiconductors aimed at the verification of unusual magnetic response in these materials.

ACKNOWLEDGMENTS

This work was supported by the Russian Science Foundation, Grant No. 20-72-10087.

[1] K. S. Novoselov, A. K. Geim, S. V. Morozov, D. Jiang, Y. Zhang, S. V. Dubonos, I. V. Grigorieva, and A. A. Firsov, Electric field effect in atomically thin carbon films, Science **306**, 666 (2004).

[2] P. Vogt, P. De Padova, C. Quaresima, J. Avila, E. Frantzeskakis, M. C. Asensio, A. Resta, B. Ealet, and G. Le Lay, Silicene: Compelling Experimental Evidence for Graphenelike Two-Dimensional Silicon, Phys. Rev. Lett. **108**, 155501 (2012).

[3] M. E. Dávila, L. Xian, S. Cahangirov, A. Rubio, and G. L. Lay, Germanene: a novel two-dimensional germanium allotrope akin to graphene and silicene, New J. Phys. **16**, 095002 (2014).

[4] A. Acun, L. Zhang, P. Bampoulis, M. Farmanbar, A. van Houselt, A. N. Rudenko, M. Lingenfelder, G. Brocks, B. Poelsema, M. I. Katsnelson, and H. J. W. Zandvliet, Germanene: the germanium analogue of graphene, J. Phys.: Condens. Matter **27**, 443002 (2015).

[5] B. Radisavljevic, A. Radenovic, J. Brivio, V. Giacometti, and A. Kis, Single-layer MoS_2 transistors, Nat. Nanotechnol. **6**, 147 (2011).

[6] R. S. Sundaram, M. Engel, A. Lombardo, R. Krupke, A. C. Ferrari, P. Avouris, and M. Steiner, Electroluminescence in single layer MoS_2, Nano Lett. **13**, 1416 (2013).

[7] O. Lopez-Sanchez, D. S. Lembke, M. Kayci, A. Radenovic, and A. Kis, Ultrasensitive photodetectors based on monolayer MoS_2, Nat. Nanotechnol. **8**, 497 (2013).

[8] L. Li, Y. Yu, G. J. Ye, Q. Ge, X. Ou, H. Wu, D. Feng, X. Chen, and Y. Zhang, Black phosphorus field-effect transistors, Nat. Nanotechnol. **9**, 372 (2014).

[9] B. Huang, G. Clark, E. Navarro-Moratalla, D. Klein, R. Cheng, K. Seyler, D. Zhong, E. Schmidgall, M. McGuire, D. Cobden, W. Yao, X. di, P. Jarillo-Herrero, and X. Xu, Layer-dependent ferromagnetism in a van der Waals crystal down to the monolayer limit, Nature (London) **546**, 270 (2017).

[10] M. Gibertini, M. Koperski, A. Morpurgo, and K. Novoselov, Magnetic 2D materials and heterostructures, Nat. Nanotechnol. **14**, 408 (2019).

[11] N. D. Mermin and H. Wagner, Absence of Ferromagnetism or Antiferromagnetism in One- or Two-Dimensional Isotropic Heisenberg Models, Phys. Rev. Lett. **17**, 1133 (1966).

[12] I. V. Kashin, V. V. Mazurenko, M. I. Katsnelson, and A. N. Rudenko, Orbitally-resolved ferromagnetism of monolayer CrI_3, 2D Mater. **7**, 025036 (2020).

[13] A. Mogulkoc, M. Modarresi, and A. N. Rudenko, Two-dimensional chromium pnictides CrX(X=P, As, Sb): Half-metallic ferromagnets with high Curie temperature, Phys. Rev. B **102**, 024441 (2020).

[14] A. Avsar, H. Ochoa, F. Guinea, B. Özyilmaz, B. J. van Wees, and I. J. Vera-Marun, Colloquium: Spintronics in graphene and other two-dimensional materials, Rev. Mod. Phys. **92**, 021003 (2020).

[15] E. E. Krasovskii, Spin-orbit coupling at surfaces and 2D materials, J. Phys.: Condens. Matter **27**, 493001 (2015).

[16] F. Reis, G. Li, L. Dudy, M. Bauernfeind, S. Glass, W. Hanke, R. Thomale, J. Schäfer, and R. Claessen, Bismuthene on a SiC substrate: A candidate for a high-temperature quantum spin Hall material, Science **357**, 287 (2017).

[17] P. Ares, J. J. Palacios, G. Abellán, J. Gómez-Herrero, and F. Zamora, Recent progress on antimonene: A new bidimensional material, Adv. Mater. **30**, 1703771 (2018).

[18] J. Ji, X. F. Song, J. Liu, Z. Yan, C. Huo, S. Zhang, M. Su, L. Liao, W. Wang, Z. Ni, Y. Hao, and H. Zeng, Two-dimensional antimonene single crystals grown by van der Waals epitaxy, Nat. Commun. **7**, 13352 (2016).

[19] P. Ares, F. Aguilar-Galindo, D. Rodríguez-San-Miguel, D. A. Aldave, S. Díaz-Tendero, M. Alcamí, F. Martín, J. Gómez-Herrero, and F. Zamora, Mechanical isolation of highly stable antimonene under ambient conditions, Adv. Mater. **28**, 6332 (2016).

[20] T. Lei, C. Liu, J.-L. Zhao, J.-M. Li, Y.-P. Li, J.-O. Wang, R. Wu, H.-J. Qian, H.-Q. Wang, and K. Ibrahim, Electronic structure of antimonene grown on Sb_2Te_3 (111) and Bi_2Te_3 substrates, J. Appl. Phys. **119**, 015302 (2016).

[21] X. Wu, Y. Shao, H. Liu, Z. Feng, Y.-L. Wang, J.-T. Sun, C. Liu, J.-O. Wang, Z.-L. Liu, S.-Y. Zhu, Y.-Q. Wang, S.-X. Du, Y.-G. Shi, K. Ibrahim, and H.-J. Gao, Epitaxial growth and air-stability of monolayer antimonene on $PdTe_2$, Adv. Mater. **29**, 1605407 (2017).

[22] C. Gibaja, D. Rodriguez-San-Miguel, P. Ares, J. Gómez-Herrero, M. Varela, R. Gillen, J. Maultzsch, F. Hauke,

A. Hirsch, G. Abellán, and F. Zamora, Few-layer antimonene by liquid-phase exfoliation, Angew. Chem. Int. Ed. **55**, 14345 (2016).

[23] D. Singh, S. K. Gupta, Y. Sonvane, and I. Lukačević, Antimonene: a monolayer material for ultraviolet optical nanodevices, J. Mater. Chem. C **4**, 6386 (2016).

[24] X. Wang, J. Song, and J. Qu, Antimonene: From experimental preparation to practical application, Angew. Chem. Int. Ed. **58**, 1574 (2019).

[25] G. Pizzi, M. Gibertini, E. Dib, N. Marzari, G. Iannaccone, and G. Fiori, Performance of arsenene and antimonene double-gate MOSFETs from first principles, Nat. Commun. **7**, 12585 (2016).

[26] H. Zhang, J. Xiong, M. Ye, J. Li, X. Zhang, R. Quhe, Z. Song, J. Yang, Q. Zhang, B. Shi, J. Yan, W. Guo, J. Robertson, Y. Wang, F. Pan, and J. Lu, Interfacial Properties of Monolayer Antimonene Devices, Phys. Rev. Appl. **11**, 064001 (2019).

[27] W. Liu and Y. Xu, *Spintronic 2D Materials: Fundamentals and Applications*, Materials Today (Elsevier Science, Amsterdam, 2019).

[28] M. Zhao, X. Zhang, and L. Li, Strain-driven band inversion and topological aspects in Antimonene, Sci. Rep. **5**, 16108 (2015).

[29] S.-Y. Zhu, Y. Shao, E. Wang, L. Cao, X.-Y. Li, Z.-L. Liu, C. Liu, L.-W. Liu, J.-O. Wang, K. Ibrahim, J.-T. Sun, Y.-L. Wang, S. Du, and H.-J. Gao, Evidence of topological edge states in buckled antimonene monolayers, Nano Lett. **19**, 6323 (2019).

[30] O. U. Aktürk, V. O. Özçelik, and S. Ciraci, Single-layer crystalline phases of antimony: Antimonenes, Phys. Rev. B **91**, 235446 (2015).

[31] A. N. Rudenko, M. I. Katsnelson, and R. Roldán, Electronic properties of single-layer antimony: Tight-binding model, spin-orbit coupling, and the strength of effective Coulomb interactions, Phys. Rev. B **95**, 081407 (2017).

[32] D. A. Prishchenko, V. G. Mazurenko, M. I. Katsnelson, and A. N. Rudenko, Gate-tunable infrared plasmons in electron-doped single-layer antimony, Phys. Rev. B **98**, 201401 (2018).

[33] A. V. Lugovskoi, M. I. Katsnelson, and A. N. Rudenko, Electron-phonon properties, structural stability, and superconductivity of doped antimonene, Phys. Rev. B **99**, 064513 (2019).

[34] M. Kurpas, P. E. Faria Jr., M. Gmitra, and J. Fabian, Spin-orbit coupling in elemental two-dimensional materials, Phys. Rev. B **100**, 125422 (2019).

[35] Y. A. Bychkov and É. I. Rashba, Properties of a 2D electron gas with lifted spectral degeneracy, JETP Lett. **39**, 78 (1984).

[36] M. Graf and P. Vogl, Electromagnetic fields and dielectric response in empirical tight-binding theory, Phys. Rev. B **51**, 4940 (1995).

[37] Y. H. Chiu, Y. H. Lai, J. H. Ho, D. S. Chuu, and M. F. Lin, Electronic structure of a two-dimensional graphene monolayer in a spatially modulated magnetic field: Peierls tight-binding model, Phys. Rev. B **77**, 045407 (2008).

[38] G. Pal, W. Apel, and L. Schweitzer, Landau level splitting due to graphene superlattices, Phys. Rev. B **85**, 235457 (2012).

[39] S. Yuan, A. N. Rudenko, and M. I. Katsnelson, Transport and optical properties of single- and bilayer black phosphorus with defects, Phys. Rev. B **91**, 115436 (2015).

[40] Z. T. Jiang, Z. T. Lv, and X. D. Zhang, Energy spectrum of pristine and compressed black phosphorus in the presence of a magnetic field, Phys. Rev. B **94**, 115118 (2016).

[41] A. Mogulkoc, M. Modarresi, and A. N. Rudenko, Effect of long-range structural corrugations on magnetotransport properties of phosphorene in tilted magnetic field, Phys. Rev. B **96**, 085434 (2017).

[42] J. L. Lado and J. Fernández-Rossier, Landau levels in 2D materials using Wannier Hamiltonians obtained by first principles, 2D Mater. **3**, 035023 (2016).

[43] X. Y. Zhou, R. Zhang, J. P. Sun, Y. L. Zou, D. Zhang, W. K. Lou, F. Cheng, G. H. Zhou, F. Zhai, and K. Chang, Landau levels and magneto-transport property of monolayer phosphorene, Sci. Rep. **5**, 12295 (2015).

[44] G. Gómez-Santos and T. Stauber, Measurable Lattice Effects on the Charge and Magnetic Response in Graphene, Phys. Rev. Lett. **106**, 045504 (2011).

[45] A. Gutiérrez-Rubio, T. Stauber, G. Gómez-Santos, R. Asgari, and F. Guinea, Orbital magnetic susceptibility of graphene and MoS_2, Phys. Rev. B **93**, 085133 (2016).

[46] L. Landau, Diamagnetismus der metalle, Z. Phys. **64**, 629 (1930).

[47] R. Peierls, Zur theorie des diamagnetismus von leitungselektronen, Z. Phys. **80**, 763 (1933).

[48] E. N. Adams, Magnetic susceptibility of a diamagnetic electron gas—The role of small effective electron mass, Phys. Rev. **89**, 633 (1953).

[49] J. Hebborn and E. Sondheimer, The diamagnetism of conduction electrons in metals, J. Phys. Chem. Solids **13**, 105 (1960).

[50] L. Roth, Theory of bloch electrons in a magnetic field, J. Phys. Chem. Solids **23**, 433 (1962).

[51] G. H. Wannier and U. N. Upadhyaya, Zero-field susceptibility of Bloch electrons, Phys. Rev. **136**, A803 (1964).

[52] P. K. Misra and L. M. Roth, Theory of diamagnetic susceptibility of metals, Phys. Rev. **177**, 1089 (1969).

[53] H. Fukuyama, A formula for the orbital magnetic susceptibility of Bloch electrons in weak fields, Phys. Lett. A **32**, 111 (1970).

[54] H. Fukuyama and R. Kubo, Interband effect on magnetic susceptibility. I. A simple two-band model, J. Phys. Soc. Jpn. **27**, 604 (1969).

[55] H. Fukuyama and R. Kubo, Interband effects on magnetic susceptibility. II. Diamagnetism of bismuth, J. Phys. Soc. Jpn. **28**, 570 (1970).

[56] A. Raoux, F. Piéchon, J.-N. Fuchs, and G. Montambaux, Orbital magnetism in coupled-bands models, Phys. Rev. B **91**, 085120 (2015).

[57] H. Matsuura and M. Ogata, Theory of orbital susceptibility in the tight-binding model: Corrections to the Peierls phase, J. Phys. Soc. Jpn. **85**, 074709 (2016).

[58] S. D. Swiecicki and J. E. Sipe, Linear response of crystals to electromagnetic fields: Microscopic charge-current density, polarization, and magnetization, Phys. Rev. B **90**, 125115 (2014).

[59] S. V. Vonsovskii, *Magnetism* (Wiley, New York, 1974).

[60] K.-T. Chen and P. A. Lee, Unified formalism for calculating polarization, magnetization, and more in a periodic insulator, Phys. Rev. B **84**, 205137 (2011).

[61] P. E. Blöchl, Projector augmented-wave method, Phys. Rev. B **50**, 17953 (1994).

[62] G. Kresse and J. Furthmüller, Efficient iterative schemes for ab initio total-energy calculations using a plane-wave basis set, Phys. Rev. B **54**, 11169 (1996).

[63] G. Kresse and J. Hafner, Ab initio molecular dynamics for liquid metals, Phys. Rev. B **47**, 558 (1993).

[64] J. P. Perdew, K. Burke, and M. Ernzerhof, Generalized Gradient Approximation Made Simple, Phys. Rev. Lett. **77**, 3865 (1996).

[65] R. Rechciński and J. Tworzydło, Landau levels of double-Weyl nodes in a simple lattice model, Acta Phys. Pol. A **130**, 1179 (2016).

[66] G. P. Arrighini, M. Maestro, and R. Moccia, Magnetic properties of polyatomic molecules. I. Magnetic susceptibility of H_2O, NH_3, CH_4, H_2O_2, J. Chem. Phys. **49**, 882 (1968).

[67] R. C. Weast, M. J. Astle, and W. H. Beyer, *CRC Handbook of Chemistry and Physics: A Ready-reference Book of Chemical and Physical Data*, 64th ed. (CRC, Boca Raton, FL, 1984).

[68] P. Selwood, *Magnetochemistry* (Read Books, UK, 2013).

[69] D. Zhang, W. Lou, M. Miao, S.-c. Zhang, and K. Chang, Interface-Induced Topological Insulator Transition in GaAs/Ge/GaAs Quantum Wells, Phys. Rev. Lett. **111**, 156402 (2013).

[70] J. Kim, S. S. Baik, S. H. Ryu, Y. Sohn, S. Park, B.-G. Park, J. Denlinger, Y. Yi, H. J. Choi, and K. S. Kim, Observation of tunable band gap and anisotropic Dirac semimetal state in black phosphorus, Science **349**, 723 (2015).

[71] K. W. Wittel and R. Manne, Atomic spin-orbit interaction parameters from spectral data for 19 elements, Theor. Chim. Acta **33**, 347 (1974).

[72] A. N. Rudenko, A. V. Lugovskoi, A. Mauri, G. Yu, S. Yuan, and M. I. Katsnelson, Interplay between in-plane and flexural phonons in electronic transport of two-dimensional semiconductors, Phys. Rev. B **100**, 075417 (2019).